A New Electrode Design Method in Piezoelectric Vibration Energy Harvesters to Maximize Output Power

Sijun Du[a], Yu Jia[a,b], Shao-Tuan Chen[a], Chun Zhao[a], Boqian Sun[c], Emmanuelle Arroyo[a] and Ashwin A. Seshia[a]

[a] Nanoscience Centre, Department of Engineering, University of Cambridge, Cambridge, CB2 1PZ, U.K.

[b] Department of Mechanical Engineering, University of Chester, Chester, CH2 4NU, U.K.

[c] Department of Precision Instrument, Tsinghua University, Beijing 100084, China.

Abstract

A resonant vibration energy harvester typically comprises of a clamped anchor and a vibrating shuttle with a proof mass. Piezoelectric materials are embedded in locations of high strain in order to transduce mechanical deformation into electrical charge. Conventional design for piezoelectric vibration energy harvesters (PVEH) usually utilizes piezoelectric materials and metal electrode layers covering the entire surface area of the cantilever with no consideration provided to examine the trade-off involved with respect to maximize output power. This paper reports on the theory and experimental verification underpinning optimization of the active electrode area in order to maximize output power. The calculations show that, in order to maximize the output power of a PVEH, the electrode should cover the piezoelectric layer from the peak strain area to a position, where the strain is a half of the average strain in all the previously covered area. With the proposed electrode design, the output power can be improved by 145% and 126% for a cantilever and a clamped-clamped beam, respectively. MEMS piezoelectric harvesters are fabricated to experimentally validate the theory.

Keywords: Energy harvesting, piezoelectric transducers, Microelectromechanical Systems (MEMS).

1 Introduction

In conventional portable electronic devices, electrochemical batteries have been dominant due to their high energy density. Although the development of ultra-low power electronics extend lifetime of such batteries, recharging and replacing them are usually inevitable for long-time sensor monitoring nodes. In certain applications, such as implantable electronics and wireless sensor nodes, charging and replacing batteries can be both impractical and costly [1]. In order to feed the needs for energy of such devices, harvesting energy from environmental kinetic vibration has attracted increasing attention as a promising alternative method in recent years [2–5]. Commonly used transduction mechanisms for vibration energy harvesting include electromagnetic, electrostatic and piezoelectric effects. Piezoelectric transducers have attracted much research interest due to its relatively high power density and compatibility with conventional micro fabrication techniques.

Piezoelectric materials are widely used in vibration energy harvesters (VEH) as mechanical-to-electrical transducers due to their relatively high power density [6], scalability and compatibility with conventional integrated circuit technologies [7–9]. To design a piezoelectric vibration energy harvester (PVEH), a cantilever with a substrate and a layer of piezoelectric material sandwiched between two metal electrode layers are widely used due to its simplicity and moderately high power density, as shown in Fig. 1. A tip mass is usually added at the free end of a cantilever to increase the output power [10]. An input vibration applied to the cantilevered PVEH causes mechanical deformation and mechanical strain on the piezoelectric material, which converts the mechanical energy to electrical energy. For piezoelectric materials, Lead-Zirconate-Titanate (PZT) is commonly used due to its relatively high piezoelectric charge constant (d_{31}, d_{33} and d_{51}); while other materials, like Zinc Oxide (ZnO) and Aluminum Nitride (AlN), are mainly used in MEMS (Microelectromechanical System) harvesters. A piezoelectric harvester can be modeled as a coupled mechanical and electrical system. While the harvester vibrates, strain (or stress) is generated in the piezoelectric material. The induced strain is then converted into electrical charge within the piezoelectric elements, resulting in a charge flow representing a current source, which charges the inherent capacitor formed by the two electrode layers. While the harvester is vibrating at or close to resonance, it can be modeled as a current source I_P connected in parallel with a capacitor C_P and a resistor R_P [11]. While the harvester is excited on a shaker driven by a sine wave signal, the current source can be written as $I_P = I_0 \sin 2\pi f_0 t$, where f_0 is the excitation frequency.

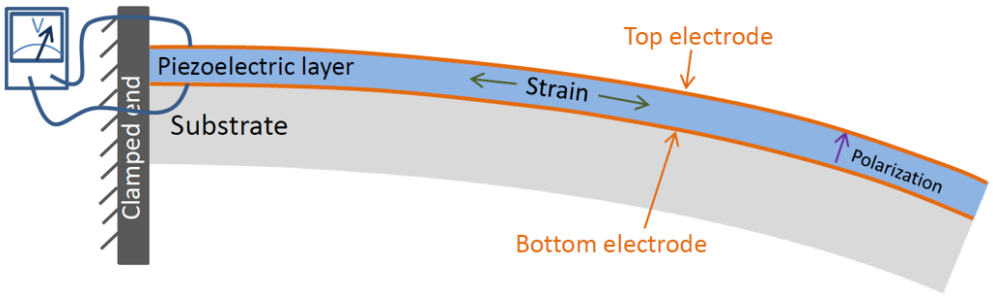

Figure 1: Simple cantilevered piezoelectric harvester

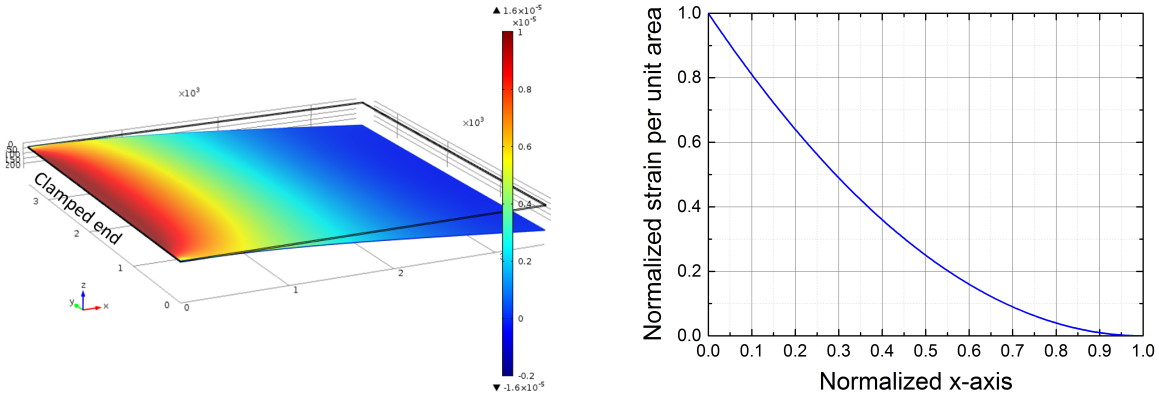

(a) (b)

Figure 2: COMSOL model of a plain cantilever shows the strain is high near the clamped end and very low near the free end. (a) COMSOL model of a cantilever with size of 3.5 mm × 3.5 mm. (b) Strain distribution on the cantilever along x-axis.

The theoretical electric power generated by a piezoelectric harvester is given as $P = \frac{1}{2} I_0^2 Z_{int}$, where I_0 is the amplitude of the current source and Z_{int} is the equivalent internal impedance of the harvester. In most of reported PVEHs, the two electrode layers usually cover all the piezoelectric layer in order to extract as much power as possible [12, 13]. However, according to the distribution of strain in the piezoelectric layer while vibrating, the volumetric strain is higher near the clamped end and very little near the free end of the cantilever, as shown in Fig. 2a. Furthermore, larger electrode area means larger C_P capacitance and smaller R_P resistance, hence smaller internal impedance. Therefore, the piezoelectric area near the clamped end should obviously be covered by electrodes due to the high strain density in this area, but the electrodes do not need to cover the free end. Because of the non-uniformly distributed strain along axis x, there should exists an optimal value for the area of electrode to maximize the generated power [14]. Although a proof mass is usually

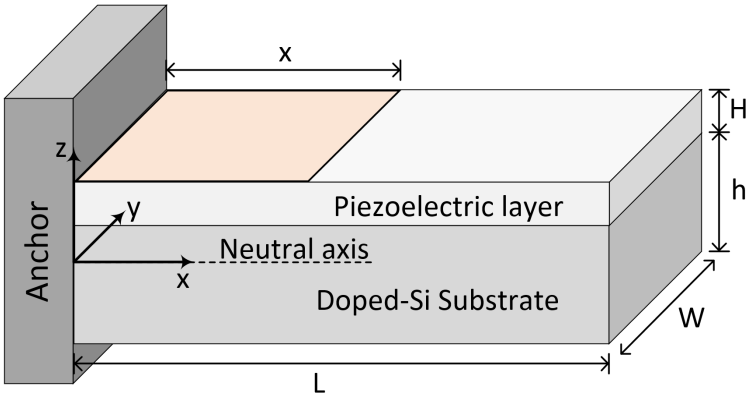

Figure 3: Cantilevered piezoelectric harvester

added at the tip of the cantilever, the maximum strain still stays at the clamped end and keeps decreasing along the x axis. Hence, the optimal electrode coverage still exists for for cantilevered PVEHs. In this paper, the optimal area of electrode layers for a maximum power output is theoretically calculated and experimentally verified with MEMS piezoelectric harvesters.

2 Modeling of a plain cantilever

In this section, a cantilevered PVEH is analyzed and its theoretical maximum output power is calculated to find an optimal electrode length to maximize the output power. Fig. 3 shows a cantilever with its geometric parameters that will be used in calculations. The length, width, thickness of the piezoelectric and substrate layers are L, W, H and h, respectively. The origin of coordinates and axis x, y and z are illustrated in the figure. The width of the electrode layer is always W while its length starting from the clamped end is a variable x, which is the value to be determined to maximize the power output. The calculation starts from the Euler-Bernoulli Beam Theory. While the cantilever is vibrating at its first mode, the displacement along z-axis for a specific point of beam at x can approximately expressed as a polynomial:

$$EI\frac{d^4\omega(x)}{dx^4} = q(t) \tag{1}$$

where E, I, $\omega(x)$ and $q(t)$ represent the Young's modulus, second moment of area of the entire cantilever, displacement of a point at x and the external excitation force per unit

length (N/m), respectively. The Young's modulus and second moment of area can be written as:

$$E = E_{piezo}\frac{H}{h+H} + E_{sub}\frac{h}{h+H} = \frac{E_{sub}h + E_{piezo}H}{h+H} \tag{2}$$

$$I = \iint z^2 dydz = \int_{-\frac{h+H}{2}}^{\frac{h+H}{2}} \int_{-\frac{W}{2}}^{\frac{W}{2}} z^2 dydz = \frac{W(h+H)^3}{12} \tag{3}$$

Assuming that the excitation force is $F = F_0 \sin\omega_0 t$ and the force is uniformly distributed along x-axis, q can be expressed as:

$$q(t) = \frac{F}{L} = \frac{F_0}{L}\sin\omega_0 t \tag{4}$$

From the Euler-Bernoulli Beam Theory in Eq. (1), $A = \frac{q}{EI}$ is set for simplifying the calculation because it is independent of x, y or z. Hence:

$$\frac{d^4\omega(x)}{dx^4} = \frac{q}{EI} = A \tag{5}$$

By integrating Eq. (5), the following expressions can be obtained:

$$\Rightarrow \frac{d^3\omega(x)}{dx^3} = Ax + C_1 \tag{6}$$

$$\Rightarrow \frac{d^2\omega(x)}{dx^2} = \frac{1}{2}Ax^2 + C_1 x + C_2 \tag{7}$$

$$\Rightarrow \frac{d\omega(x)}{dx} = \frac{1}{6}Ax^3 + \frac{1}{2}C_1 x^2 + C_2 x + C_3 \tag{8}$$

$$\Rightarrow \omega(x) = \frac{1}{24}Ax^4 + \frac{1}{6}C_1 x^3 + \frac{1}{2}C_2 x^2 + C_3 x + C_4 \tag{9}$$

According to Dirichlet Boundary Conditions, initial conditions can be set as $\omega' = \omega = 0$ at the clamped end and, $\omega''' = \omega'' = 0$ at the free end. Therefore, the following four equations is obtained:

$$\begin{aligned} \frac{d^3\omega(L)}{dx^3} &= 0 \\ \frac{d^2\omega(L)}{dx^2} &= 0 \\ \frac{d\omega(0)}{dx} &= 0 \\ \omega(0) &= 0 \end{aligned} \tag{10}$$

With the four equations in Eq. (10), it can be solved that $C_1 = -AL$, $C_2 = \frac{1}{2}AL^2$, $C_3 = 0$, $C_3 = 0$. Replacing the parameters in Eqs. (9) and (7):

$$\omega(x) = \frac{1}{24}Ax^4 - \frac{1}{6}ALx^3 + \frac{1}{4}AL^2x^2 \tag{11}$$

$$\frac{d^2\omega(x)}{dx^2} = \frac{1}{2}Ax^2 - ALx + \frac{1}{2}AL^2 \tag{12}$$

For a symmetrical bending, the tensile stress experienced by the beam can be expressed as:

$$\sigma_{(x,y,z)} = \frac{Mz}{I} \tag{13}$$

where M is the bending moment which is given by $M = -EI\frac{d^2\omega(x)}{dx^2}$, I is the second moment of area calculated in Eq. (3), so the stress can be written as:

$$\begin{aligned} \sigma_{(x,y,z)} = -zE\frac{d^2\omega(x)}{dx^2} &= -zE(\frac{1}{2}Ax^2 - ALx + \frac{1}{2}AL^2) \\ &= -z\frac{q}{I}(\frac{1}{2}x^2 - Lx + \frac{1}{2}L^2) \end{aligned} \tag{14}$$

Where $\sigma_{(x,y,z)}$ is the stress per unit area ($\mathrm{N/m^2}$) and its variable z starts from the origin of coordinates along the axis z, as shown in Fig. 3. In order to convert the kinetic energy to electrical energy, the piezoelectric charge constant d_{31} needs to be used. Therefore, the amount of charge generated by the strain is expressed as:

$$Q_{(x,y,z)} = d_{31}\sigma_{(x,y,z)} = -zd_{31}\frac{q}{I}(\frac{1}{2}x^2 - Lx + \frac{1}{2}L^2) \tag{15}$$

This is the charge generated per unit area $dxdy$ in the piezoelectric material. In order to calculate the total charge across the two electrode layers $z_{bottom} = \frac{h-H}{2}$ and $z_{top} = \frac{h+H}{2}$ (assuming the substrate is thicker than the piezoelectric layer, $h > H$), Eq. (15) needs to be integrated along x, y:

$$Q_{total} = \int_0^x \int_o^W Q_{(x,y,z)} dydx \Big|_{z=\frac{h-H}{2}}^{z=\frac{h+H}{2}} \tag{16}$$

$$\begin{aligned} \Rightarrow Q_{total} &= \int_0^x \int_o^W -Hd_{31}\frac{q_{(t)}}{I}(\frac{1}{2}x^2 - Lx + \frac{1}{2}L^2)dydx \\ &= -q_{(t)}d_{31}\frac{WH}{I}(\frac{1}{6}x^3 - \frac{1}{2}Lx^2 + \frac{1}{2}L^2x) \end{aligned} \tag{17}$$

According to equation 4, the excitation force $q_{(t)}$ is a function of time $q = \frac{F_0}{L}\sin\omega_0 t$. Hence, the generated charge is:

$$Q_{total} = -d_{31}\frac{F_0}{L}\frac{WH}{I}(\frac{1}{6}x^3 - \frac{1}{2}Lx^2 + \frac{1}{2}L^2x)\sin\omega_0 t \tag{18}$$

A piezoelectric harvester can be modeled as a current source I_P in parallel with a capacitor C_P and a resistor R_P. The capacitor C_P together with the resistor R_P can be considered as the internal impedance Z_P of the harvester. In order to calculate the generated power by the harvester, it is needed to calculate I_P, C_P and R_P. The calculation starts from determining I_P. As the total charge between the two electrodes is found in Eq. (18), the generated current can be deduced by calculating the derivative of charge to time.

$$\begin{aligned} I_P = \frac{dQ_{total}}{dt} &= -d_{31}\frac{F_0\omega_0}{L}\frac{WH}{I}(\frac{1}{6}x^3 - \frac{1}{2}Lx^2 + \frac{1}{2}L^2x)cos(\omega_0 t) \\ &= I_0 cos(\omega_0 t) \end{aligned} \tag{19}$$

$$\Big(with\ I_0 = -d_{31}\frac{F_0\omega_0}{L}\frac{WH}{I}(\frac{1}{6}x^3 - \frac{1}{2}Lx^2 + \frac{1}{2}L^2x)\Big)$$

The capacitance and resistance can be expressed in Eq. (20) and Eq. (21) according to the geometric dimensions of the electrode layer.

$$C_P = \varepsilon_r\varepsilon_0\frac{xW}{H} \tag{20}$$

$$R_P = \rho \frac{H}{xW} \tag{21}$$

In the equations, ε_r and ε_0 represent dielectric constant of piezoelectric material and electric constant, respectively; ρ is the electrical resistivity of the piezoelectric material. Therefore, the internal impedance can be expressed as:

$$Z_p = C_P // R_P = |\frac{\frac{R_P}{2\pi C_P}}{R_P + \frac{1}{j\omega_0 C_P}}| = \frac{\rho}{\sqrt{1+\omega_0^2 \varepsilon_r^2 \varepsilon_0^2 \rho^2}} \frac{H}{xW} \tag{22}$$

The generated power by the PVEH is:

$$P_0 = \frac{1}{2} I_0^2 Z_p \tag{23}$$

$$\Rightarrow P_0 = \frac{1}{2}\Big(- d_{31} \frac{F_0 \omega_0}{L} \frac{WH}{I} (\frac{1}{6}x^3 - \frac{1}{2}Lx^2 + \frac{1}{2}L^2 x)\Big)^2 \frac{\rho}{\sqrt{1+\omega_0^2 \varepsilon_r^2 \varepsilon_0^2 \rho^2}} \frac{H}{xW} \tag{24}$$

$$\Rightarrow P_0 = d_{31}^2 F_0^2 \omega_0^2 \frac{WH^3}{2I^2 L^2} \frac{\rho}{\sqrt{1+\omega_0^2 \varepsilon_r^2 \varepsilon_0^2 \rho^2}} x(\frac{1}{6}x^2 - \frac{1}{2}Lx + \frac{1}{2}L^2)^2 \tag{25}$$

From Eq. (3), the expression of the second moment of area is $I = \frac{W(h+H)^3}{12}$, Hence:

$$\begin{gathered} P_0 = B(\frac{1}{36}x^5 - \frac{1}{6}Lx^4 + \frac{5}{12}L^2 x^3 - \frac{1}{2}L^3 x^2 + \frac{1}{4}L^4 x) \\ \Big(with\ B = d_{31}^2 F_0^2 \omega_0^2 \frac{72H^3}{WL^2(h+H)^6}\ \frac{\rho}{\sqrt{1+\omega_0^2 \varepsilon_r^2 \varepsilon_0^2 \rho^2}}\Big) \end{gathered} \tag{26}$$

The expression of the generated electrical power by the piezoelectric harvester is given in Eq. (26) and it is a function of x, which is the length of the electrode layer. The normalized power is plotted in the dash line in Fig. 4 and the horizontal axis is the normalized x axis along the cantilever where x=0 is the anchor and x=1 is the free end. The dash-dot line in the figure shows the normalized strain along the x-axis and its expression is given in Eq. (14). It can be seen that the output electrical power of a plain cantilever reaches its peak at

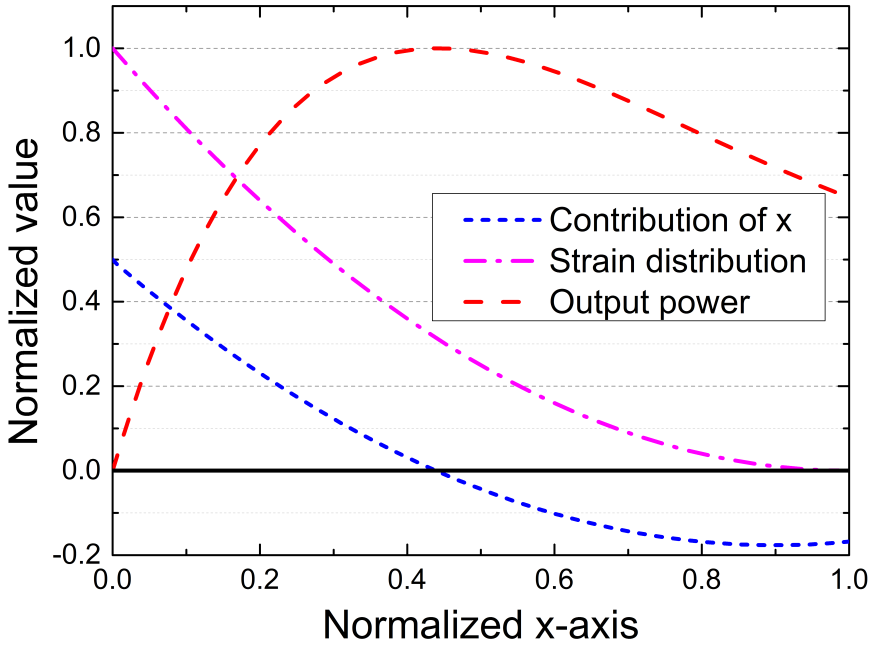

Figure 4: Simulation results

$x \approx 0.44L$, which means the electrode layer covering 44% of the cantilever from the clamped end maximizes the power. Another line named "Contribution of x" (short-dash) will be explained in the next section and it is the result using another new method, which works for any designs.

3 Modeling of a structure with arbitrary strain distribution

In order to increase the generated power and adjust frequency bandwidth of PVEHs, different designs have been proposed. Tip masses are added in many cantilevered harvesters to tune the natural frequency and increase output power [15–17]. Other designs, such as clamped-clamped beams [18, 19] and more complicated designs [20, 21] have also been presented in recent years for output power and bandwidth enlargement reasons. The electrode design rule for a plain cantilever is calculated in the previous section; however, it is important to find a generalized rule on designing the electrode layers for different structures of PVEHs to maximize the output power.

This section presents a generalized method on strain distribution analysis to determine

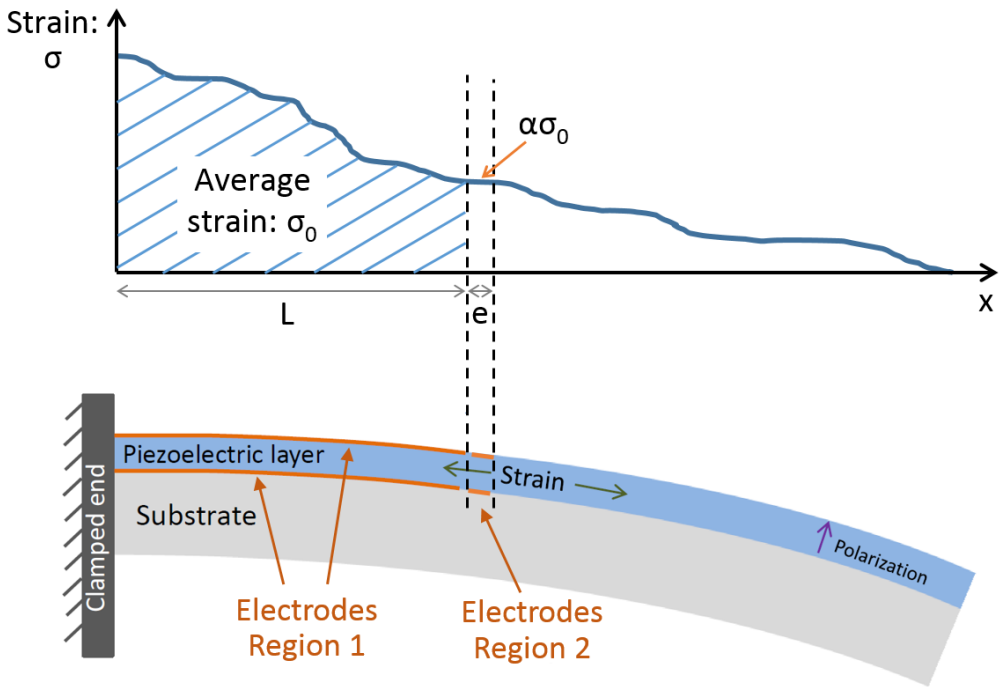

Figure 5: A piezoelectric vibration energy harvester with arbitrary decreasing strain along axis x (L is the length of the electrode region 1 and e is the length of an extract electrode region 2, where $e \ll L$. the average strain in the region 1 is noted as σ_0, α is a factor between 0 and 1 and $\alpha\sigma_0$ is the strain for the small region 2).

the optimal electrode coverage for any kind of structures. Fig. 5 shows a piezoelectric harvester, in which the strain distributed along x is assumed to be arbitrary and decreasing. The reason of using the arbitrary strain distribution is to make the proposed method suitable for any kind of structures, such as cantilevers, clamp-clamp beams, etc.

The highest strain is located near the clamped end. First, it is assumed that the electrode layer covers the region 1 of length L. The region 1 is then increased by a very small region 2, with length e, where $e \ll L$. The analysis becomes calculating if the output power of regions 1+2 is greater or less than that of the single region 1; so that it can be found if the region 2 contributes to increase the output power and if the region 1 is the optimal electrode coverage.

It is assumed that σ_0 is the average strain per unit length in the region 1 and $\alpha\sigma_0$ is the strain per unit length in region 2, where α satisfies $0 < \alpha < 1$. In the following parts, the output power values generated by the electrode coverage of region 1 and regions 1+2 are separately calculated and compared in order to find the power contribution of the additional

electrode area in the region 2.

3.1 Output power with electrode covering region 1

As the average strain per unit length in the region 1 is σ_0, the total strain in this region is expressed as:

$$\sigma_1 = \sigma_0 L \sin \omega t \tag{27}$$

where ω is the excitation frequency. The total charge generated in region 1 is:

$$Q_1 = d_{31}\sigma_0 L \sin \omega t \tag{28}$$

The equivalent current source can be written as:

$$I_1 = \frac{\mathrm{d}Q_1}{\mathrm{d}t} = \omega d_{31}\sigma_0 L \cos \omega t \tag{29}$$

Assuming the inherent capacitance per unit length of the electrode is C_0, the capacitance for region 1 is $C_1 = C_0 L$. The internal impedance for region 1 while the PVEH is vibrating is expressed as:

$$|Z_1| = \frac{1}{\omega C_0 L} \tag{30}$$

In the previous section, a PVEH is modeled to be a current source in parallel with a capacitor C_P and a resistor R_P. As the impedance of R_P is usually significantly higher than that of C_P, the resistor R_P can be neglected to facilitate the calculations. Therefore, according to the equations Eq. (29) and Eq. (30), the output power while the electrode only covers the region 1 is calculated as:

$$P_1 = \frac{\omega^2 d_{31}^2 \sigma_0^2 L^2}{2} \frac{1}{\omega C_0 L} = \frac{\omega d_{31}^2 \sigma_0^2 L}{2C_0} \tag{31}$$

3.2 Output power with electrode covering regions 1+2:

After obtaining the output power with electrode only covering the region 1, the small region 2 is added in this section to see how this additional electrode coverage contributes to the output power. As the strain per unit length in the region 2 is expressed as $\alpha\sigma_0$, which is shown in Fig. 5, the total strain in regions 1+2 is:

$$\sigma_{1+2} = \sigma_0 L \sin \omega t + \alpha\sigma_0 e \sin \omega t \tag{32}$$

The total charge generated in regions 1+2 can be expressed as:

$$Q_{1+2} = (L + \alpha e)\sigma_0 d_{31} \sin \omega t \tag{33}$$

Hence, the equivalent current source for the electrode covering regions 1+2 is:

$$I_{1+2} = \frac{\mathrm{d}Q_{1+2}}{\mathrm{d}t} = \omega(L + \alpha e)\sigma_0 d_{31} \cos \omega t \tag{34}$$

The inherent capacitance and internal impedance for regions 1+2 are expressed as:

$$C_{1+2} = C_0(L + e) \Rightarrow |Z_{1+2}| = \frac{1}{\omega C_0(L + e)} \tag{35}$$

According to equations Eq. (34) and Eq. (35), the output power for a PVEH with electrode covering region 1+2 is:

$$P_{1+2} = \frac{\omega^2 d_{31}^2 \sigma_0^2 (L + \alpha e)^2}{2} \frac{1}{\omega C_0(L + e)} = \frac{\omega d_{31}^2 \sigma_0^2 (L + \alpha e)^2}{2C_0(L + e)} \tag{36}$$

3.3 Contribution analysis of additional electrode coverage in region 2

In order to find how the additional electrode in the region 2 contributes to the total output power of the PVEH, the output power calculated in equations Eq. (31) and Eq. (36) are compared:

$$
\begin{aligned}
P_{1+2} &> P_1 \\
\Rightarrow \frac{\omega d_{31}^2 \sigma_0^2 (L+\alpha e)^2}{2C_0(L+e)} &> \frac{\omega d_{31}^2 \sigma_0^2 L}{2C_0} \\
\Rightarrow \frac{(L+\alpha e)^2}{L+e} &> L \\
\Rightarrow L^2 + \alpha^2 e^2 + 2L\alpha e &> L^2 + Le \\
\Rightarrow \alpha^2 \frac{e}{L} + 2\alpha &> 1
\end{aligned}
\tag{37}
$$

As the region 2 is assumed to be much smaller than the region 1 ($e \ll L$); hence, $e/L \approx 0$. After applying this approximation into the equation Eq. (37), the variable α can be found as:

$$
\alpha > 0.5 \tag{38}
$$

The above result implies that the additional electrode in region 2 will increase the output power of the PVEH only if the unit strain in this region is greater than a half of the average strain in region 1. If the unit strain at the edge of the region 1 equals to the half of the average strain in region 1, the existing electrode is the optimal coverage outputting maximum electrical power and any additional electrode will decrease the power. Hence, in order to maximize the output power of a PVEH, the electrode layer should cover from the peak strain end to a position, where the unit strain in this position is a half of the average strain of the area covered by the electrode layer.

Fig. 4 shows the simulation results for a plain cantilevered piezoelectric energy harvester. The short-dash line is the normalized strain $\sigma(x)$ per unit length along the x axis, which is expressed in Eq. (14). The dash-dot line represents the contribution to the total output power of an additional region 2 at the position x. This line is plotted according to the function $Contribution = \sigma(x) - \frac{\int_0^x \sigma(x)\,\mathrm{d}x}{2}$, which represents the difference between the unit strain at x and a half of the average strain before x. The strain $\sigma(x)$ in the function is given in Eq. (14). This function is formed according to the result obtained in the equation Eq. (38). From the dash-dot line, it can be seen that the contribution of electrode at a specific x keeps positive for $x < 0.44$ and it goes to negative for $x > 0.44$, which implies that 44% is the optimal electrode coverage for a plain cantilevered PVEH. This result matches the peak output power of the dash line, which is calculated using Euler-Bernoulli Beam Theory method.

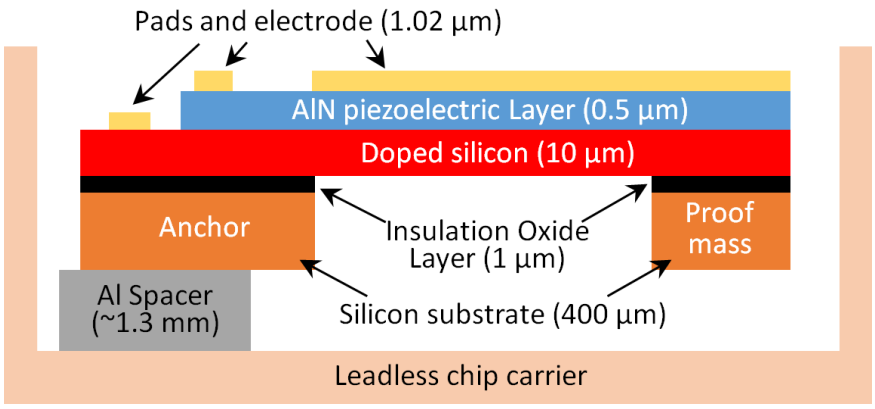

Figure 6: MEMS device fabrication process

In the next section, two MEMS devices have been fabricated and experimentally tested to validate the results obtained in the calculations.

4 Experiments

In this section, two PVEHs of different structures are fabricated in MEMS process to experimentally validate the theoretical calculations. Both MEMS devices are fabricated with MEMSCAP piezoMUMPs technology, which involves a 400 µm silicon substrate, a 10 µm doped silicon layer, a 0.5 µm AlN (Aluminum Nitride) piezoelectric layer and a 1.02 µm top electrode layer. The process is illustrated in Fig. 6. The MEMS device to be tested is clamped in a chip socket, which is fixed on a shaker. The experimental setup is shown in Fig. 7. The shaker (LDS V406 M4-CE) is excited at the natural frequency of each MEMS device and driven by a sine wave from a function generator (Agilent Technologies 33250A 80 MHz waveform generator) amplified by a power amplifier (LDS PA100E Power Amplifier). A variable resistor box is employed as the load and the output electrical power is calculated from the measurement by an oscilloscope.

4.1 MEMS plain cantilever

The first device to be tested is a plain cantilever without a proof mass, which is shown in Fig. 8. The size of the cantilever is 3.5 mm × 3.5 mm and the electrode layer is split into 8 segments. From region 1 to region 8, they sequentially occupy 20%, 10%, 10%, 10%, 10%, 10%, 10% and 20% respectively, of the total length of the cantilever. The device in the

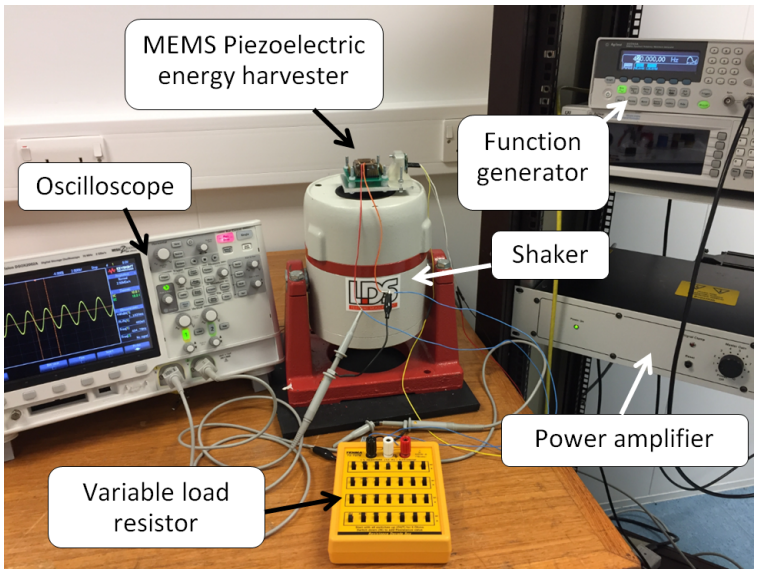

Figure 7: Experimental setup

figure contains 12 electrode pads where there are 8 pads for 8 regions and 4 pads for ground. The natural frequency of the cantilever is 1208 Hz and the input acceleration level in the experiment is 0.5 g.

Experiments are performed in two steps. The first step is using the theoretical result obtained in Eq. (38) to estimate the optimum electrode coverage: the open-circuit voltage of each individual electrode is measured to detect the electrode on which the voltage is half of the average voltage on the previous electrodes. The second step consists in gradually increasing the electrode area by adding regions from 1 to 8 and measuring the output power to find the optimal electrode coverage. For each measurement point, the load resistor is adjusted to match the internal impedance. The result is then compared with step 1 to validate the theoretical calculations.

Table 1 shows the measured open-circuit voltage and contribution for each individual region from 1 to 8 and the measured output power while gradually adding the electrodes from 1 to 8. The results are plotted in Fig. 9, where the x axis is presented in Fig. 8. The measured values of open voltage and contribution values for the eight regions correspond to the positions at the centers of the regions, which are x = 0.1, 0.25, 0.35, 0.45, 0.55, 0.65, 0.75 and 0.9. The contribution value, for region 6 for example, is the voltage value at region 6 minus the half of the average value of all previous regions. This is expressed as: $Contribution_6 = V_6 - \frac{1}{2}\frac{\sum_{i=1}^{5} V_i}{5}$. Although the condition in equation Eq. (38) is calculated with strain, open-circuit voltage is used to represent the strain here.This is because the

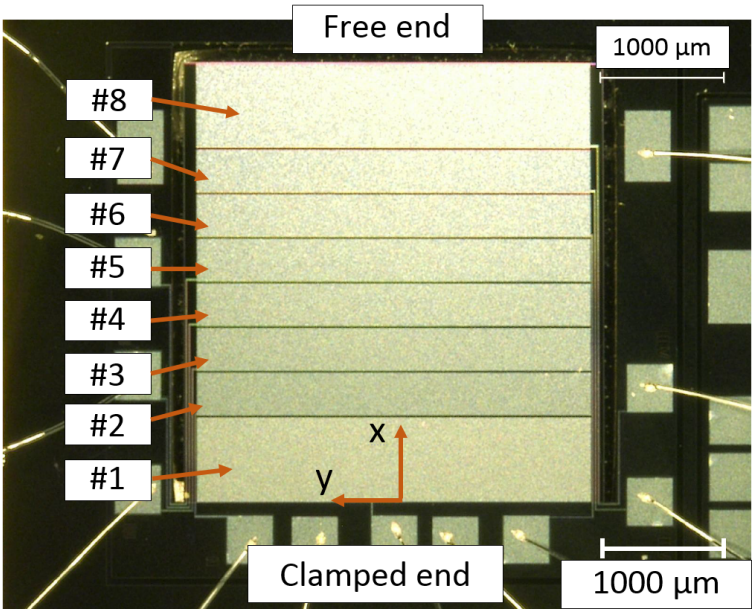

Figure 8: Microscopic view of a MEMS plain cantilevered PVEH

open-circuit voltage is proportional to the generated charge, which is proportional to the total strain in a region. Positive values in the "Power contribution" column means adding these regions into the electrode can increase the output power. It can be seen from the figure that the "contribution" line crosses zero at around x = 0.48, which means a 48% electrode coverage is the theoretical optimal electrode side to maximize the output power. The peak power measured in step 2 is found at around 50% or slightly smaller if applying a polynomial fitting, which closely matches the results read from the contribution line. The mismatching between the theoretical and experimental results can be due to the parasitic capacitance of the pads and the Euler-Bernoulli beam theory employed in a cantilever.

4.2 MEMS clamped-clamped beam

The second MEMS device to be tested is shown in Fig. 10. This is a clamped-clamped beam PVEH where the left and right sides of the beam are clamped and a proof mass is suspended in the center. The size of the clamped-clamped beam is 8 mm × 2 mm. The middle rectangular area in black is the proof mass with size of 1.5 mm × 2 mm. The thickness of the proof mass is around 400 µm, as shown in Fig. 6. In two large segmented white rectangles on both sides of the middle proof mass, the silicon substrate is etched. They are covered by the segmented top metal layer. For each side of the structure, the electrode layer is segmented

Table 1: Measured open-circuit voltage and output power contribution for each region of the MEMS cantilever PVEH (frequency: 1208 Hz, acceleration: 0.5 g)

Region	Capacitance (nF)	Open-circuit voltage (mV)	Contribution to power	Output power (nW)
#1	0.464	970	485.0	140
#2	0.294	661	176.0	180.6
#3	0.27	507	99.3	214.1
#4	0.273	389	32.7	222
#5	0.272	291	-24.9	213.2
#6	0.272	193	-88.8	199.5
#7	0.272	92	-158.9	189.6
#8	0.472	23	-198.6	153.6

into 19 pieces, hence 38 pieces in total for both sides. As the strain distribution for both sides is theoretically symmetric, only the 19 electrode pieces on the left side of the beam are routed out to 19 pads. The other 19 pieces on the right side are not connected and they are designed to keep the mechanical symmetry of the device. The electrode regions to be tested are labeled from 1 to 19.

Similar to the previous experiments on the plain cantilever, the measurements on this device are also performed in two similar steps. In the first step, the clamped-clamped beam is excited at its natural frequency 1430 Hz under an excitation level of 0.5 g. The optimal electrode is estimated according to the theoretical calculations, by measuring the open-circuit voltage for each of the 19 regions. In the send step, the output power is directly measured as a function of the electrode length, to validation the results obtained in step 1. In comparison with a cantilever, the strain distribution in a clamped-clamped beam is not continuously decreasing along the length of the beam. From region 1, it decreases until it attains zero in the near center (region 10) and increase until region 19. Taking that into account, the step 2 of experiments is performed in two sub-steps: increasing the electrode from 1 to 10 in a first part, and from 19 to 11 in a second part. Hence, the experiments are performed by considering the regions 1 to 19 as two parts: one part from 1 to 10 and the other part 19 to 11.

Table 2 shows the measured open-circuit voltage and contribution value for each of the 19 regions. It also shows the output power for the two parts of electrode regions and the

Table 2: Measured open-circuit voltage and output power contribution for each region of the MEMS clamped-clamped beam PVEH (frequency: 1430 Hz, acceleration: 0.5 g)

Region	Capacitance (nF)	Open-circuit voltage (mV)	Contribution to power	Output power (nW)
#1	0.111	1210	605	91.22
#2	0.118	1070	465	172.15
#3	0.113	944	374	219.75
#4	0.113	821	283.7	259.44
#5	0.113	677	171.4	282.84
#6	0.113	544	71.8	293.13
#7	0.115	410	-28.8	297.07
#8	0.116	272	-133.4	287.93
#9	0.117	149	-222.8	271.24
#10	0.119	23	-315.7	250.16
#11	0.123	46	-293.6	230.36
#12	0.121	180	-195.3	250.67
#13	0.12	331	-79.3	265.61
#14	0.121	478	33.5	274.33
#15	0.117	606	126.1	259.50
#16	0.113	749	234	233.68
#17	0.119	890	340	212.58
#18	0.121	1020	430	164.35
#19	0.119	1180	590	93.00

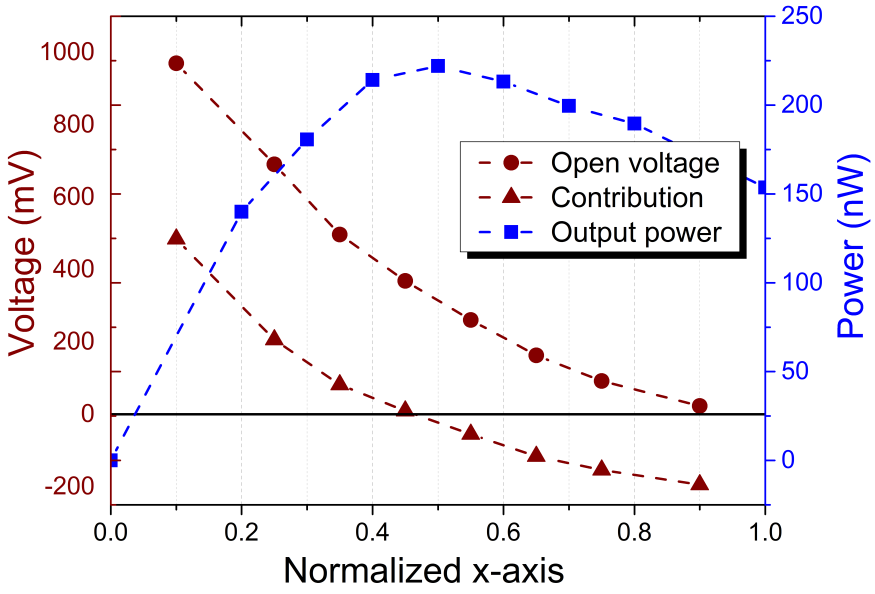

Figure 9: Measured results for MEMS plain cantilevered PVEH

results are plotted in Fig. 11. The formula used to calculate the contribution values is the same as the one used in the previous cantilever measurements; however, the contribution values in the left and right parts are calculated individually from regions 1 and 19. According to the figure, the contribution value crosses zero between regions 6 and 7, and then again between regions 13 and 14. The results indicate that the regions from 7 to 13 have negative contributions to the output and they should not be added into electrode design.

Regarding the left part of the output power, it can be seen that it reaches a peak at region 7, and adding any further regions decreases the output power. Similarly, for the right part, gradually increasing the electrode from the region 19 increases the output power until it reaches its peak at the region 14, and any additional regions will decease the power from the right part. Therefore, the optimal electrode layer for this particular clamped-clamped beam should cover the regions 1 to 7 and regions 14 to 19. The two peaks of the output power closely match the two points where the contribution line crosses zero, and thus validate the theoretical calculations, found in equation (38), for this clamped-clamped beam.

The maximum output power for all the regions 1 to 19 is the sum of the left and right peak power points and the output power of the whole clamped-clamped beam PVEH should be further multiplied by 2 as there are another identical 19 electrode regions on the other side of the structure, as shown in Fig. 10

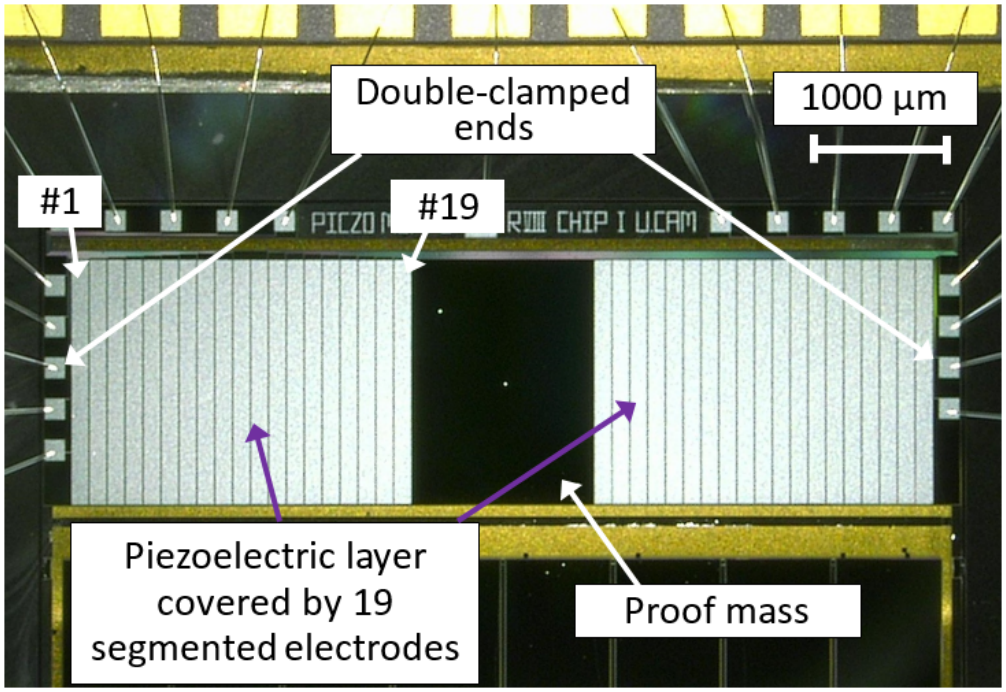

Figure 10: Microscopic view of a MEMS clamped-clamped beam PVEH with a centered proof mass

4.3 Discussion

According to the results on the plain cantilever in Fig. 9, if the electrode covers the entire area (100% coverage), the resulting output power is 153.6 nW. However, the proposed design on the electrode increases the power to 222 nW with an output power improvement of 144.5%. For the clamped-clamped beam in Fig. 11, the total estimated output power for the entire device, while the electrode cover all the 19 regions, is 936 nW (twice of the sum of power at the regions 10 and 11) . If the electrode coverage is optimized, the output power can achieve 1178 nW (twice of the sum of power at the two peaks). The power improvement is around 126%.

5 Conclusion

In this paper, theoretical calculations were performed to find an optimal electrode coverage for maximizing output power of a PVEH. The results show that maximizing the electrode layer does not always increase output power; in the contrast, power can be reduced if the low-strain area is covered. According to the calculations, the low-strain area is defined as

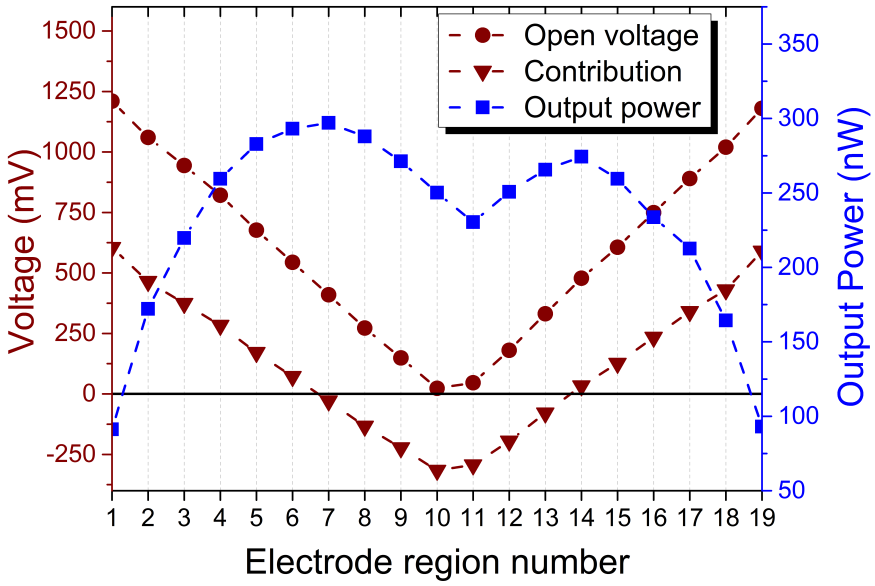

Figure 11: Measured results for MEMS clamped-clamped beam PVEH

an area, where the strain is less than a half of the average strain in other high strain areas. This result can also be interpreted as the optimal electrode coverage is the electrode layer covering from the peak strain area to a place, where the strain is equal to a half of the average strain in all the previously covered high-strain area. With the proposed electrode design method, the output power can be improved by 145% and 126% for the tested cantilever and clamped-clamped beam PVEHs, respectively. The theoretical calculations are validated with measured results based on a MEMS cantilevered harvester and a MEMS clamped-clamped beam harvester and the discrepancy between the theoretical and experimental results were explained. The reason of the using two different MEMS devices is to validate that the proposed method can be applied to different structures with different strain distributions.

According to the results of this paper, while designing a piezoelectric vibration energy harvester (PVEH) at either macroscopic or MEMS scale, the active electrode layer does not necessarily need to cover the entire piezoelectric layer. Before fabricating the PVEHs, simulation results on the strain distribution can be used to find the approximate optimal electrode coverage and apply this consideration in the design to maximize the output power. This design approach can also be applied to other structural topologies and mode shapes for piezoelectric vibration energy harvesters.

Funding: This work was supported by the Engineering and Physical Sciences Research Council (EPSRC) [grant number EP/L010917/1].

References

[1] M. Belleville, H. Fanet, P. Fiorini, P. Nicole, M. J. M. Pelgrom, C. Piguet, R. Hahn, C. Van Hoof, R. Vullers, M. Tartagni, and E. Cantatore, "Energy autonomous sensor systems: Towards a ubiquitous sensor technology," *Microelectronics Journal*, vol. 41, no. 11, pp. 740–745, 2010.

[2] S. P. Beeby, R. Torah, M. Tudor, P. Glynne-Jones, T. O'Donnell, C. Saha, and S. Roy, "A micro electromagnetic generator for vibration energy harvesting," *Journal of Micromechanics and microengineering*, vol. 17, no. 7, p. 1257, 2007.

[3] A. Khaligh, Z. Peng, and Z. Cong, "Kinetic energy harvesting using piezoelectric and electromagnetic technologies 2014;state of the art," *Industrial Electronics, IEEE Transactions on*, vol. 57, no. 3, pp. 850–860, 2010.

[4] G. D. Szarka, B. H. Stark, and S. G. Burrow, "Review of power conditioning for kinetic energy harvesting systems," *Power Electronics, IEEE Transactions on*, vol. 27, no. 2, pp. 803–815, 2012.

[5] P. D. Mitcheson, E. M. Yeatman, G. K. Rao, A. S. Holmes, and T. C. Green, "Energy harvesting from human and machine motion for wireless electronic devices," *Proceedings of the IEEE*, vol. 96, no. 9, pp. 1457–1486, 2008.

[6] G. Tang, B. Yang, J.-q. Liu, B. Xu, H.-y. Zhu, and C.-s. Yang, "Development of high performance piezoelectric d33 mode mems vibration energy harvester based on pmn-pt single crystal thick film," *Sensors and Actuators A: Physical*, vol. 205, no. 0, pp. 150–155, 2014.

[7] N. Elvin and A. Erturk, *Advances in energy harvesting methods*. Springer Science & Business Media, 2013.

[8] S. Du, Y. Jia, C. D. Do, and A. A. Seshia, "An efficient sshi interface with increased input range for piezoelectric energy harvesting under variable conditions," *IEEE Journal of Solid-State Circuits*, vol. 51, no. 11, pp. 2729–2742, 2016.

[9] M. Han, Q. Yuan, X. Sun, and H. Zhang, "Design and fabrication of integrated magnetic mems energy harvester for low frequency applications," *Microelectromechanical Systems, Journal of*, vol. 23, no. 1, pp. 204–212, 2014.

[10] W. G. Li, S. He, and S. Yu, "Improving power density of a cantilever piezoelectric power harvester through a curved l-shaped proof mass," *IEEE Transactions on Industrial Electronics*, vol. 57, no. 3, pp. 868–876, 2010.

[11] S. J. Roundy, "Energy scavenging for wireless sensor nodes with a focus on vibration to electricity conversion," Thesis, 2003.

[12] M. Stewart, P. M. Weaver, and M. Cain, "Charge redistribution in piezoelectric energy harvesters," *Applied Physics Letters*, vol. 100, no. 7, p. 073901, 2012.

[13] K. Wasa, T. Matsushima, H. Adachi, I. Kanno, and H. Kotera, "Thin-film piezoelectric materials for a better energy harvesting mems," *Microelectromechanical Systems, Journal of*, vol. 21, no. 2, pp. 451–457, 2012.

[14] S. Du, Y. Jia, and A. Seshia, "Maximizing output power in a cantilevered piezoelectric vibration energy harvester by electrode design," *Journal of Physics: Conference Series*, vol. 660, no. 1, p. 012114, 2015.

[15] H. Liu, C. J. Tay, C. Quan, T. Kobayashi, and C. Lee, "Piezoelectric mems energy harvester for low-frequency vibrations with wideband operation range and steadily increased output power," *Microelectromechanical Systems, Journal of*, vol. 20, no. 5, pp. 1131–1142, 2011.

[16] R. Andosca, T. G. McDonald, V. Genova, S. Rosenberg, J. Keating, C. Benedixen, and J. Wu, "Experimental and theoretical studies on mems piezoelectric vibrational energy harvesters with mass loading," *Sensors and Actuators A: Physical*, vol. 178, no. 0, pp. 76–87, 2012.

[17] H. Wu, L. Tang, Y. Yang, and C. K. Soh, "A novel two-degrees-of-freedom piezoelectric energy harvester," *Journal of Intelligent Material Systems and Structures*, p. 1045389X12457254, 2012.

[18] X. Xiong and S. O. Oyadiji, "Modal optimization of doubly clamped base-excited multilayer broadband vibration energy harvesters," *Journal of Intelligent Material Systems and Structures*, p. 1045389X14551433, 2014.

[19] A. Hajati, S. P. Bathurst, H. J. Lee, and S. G. Kim, "Design and fabrication of a nonlinear resonator for ultra wide-bandwidth energy harvesting applications," in *Micro*

Electro Mechanical Systems (MEMS), 2011 IEEE 24th International Conference on, Conference Proceedings, pp. 1301–1304.

[20] S. Leadenham and A. Erturk, "Nonlinear m-shaped broadband piezoelectric energy harvester for very low base accelerations: primary and secondary resonances," *Smart Materials and Structures*, vol. 24, no. 5, p. 055021, 2015.

[21] D. J. Apo, M. Sanghadasa, and S. Priya, "Low frequency arc-based mems structures for vibration energy harvesting," in *Nano/Micro Engineered and Molecular Systems (NEMS), 2013 8th IEEE International Conference on*, Conference Proceedings, pp. 615–618.